JACS
JOURNAL OF THE AMERICAN CHEMICAL SOCIETY
pubs.acs.org/JACS
Article

Pinwheel-like Curved Aromatics from the Cyclotrimerization of Strained Alkyne Cycloparaphenylenes

Tara D. Clayton,[§] Julia M. Fehr,[§] Tavis W. Price, Lev N. Zakharov, and Ramesh Jasti*

Cite This: J. Am. Chem. Soc. 2024, 146, 30607−30614
Read Online
ACCESS | Metrics & More | Article Recommendations | Supporting Information

ABSTRACT: Carbon nanomaterials composed of curved aromatics, such as carbon nanotubes, are difficult to selectively synthesize and modify precisely. Smaller molecular fragments of curved nanomaterials, such as cycloparaphenylenes, benefit from the precision of bottom-up synthesis, however, efforts to expand the curved molecular framework into even larger structures often rely on restrictive early stage synthetic strategies or difficult to control polymerizations. In this work we report a high yielding, strain-promoted, late-stage modification of a series of [*n* + 1]CPPs. We show that the conversion of these [*n* + 1]CPPs into soluble, pinwheel-like multipore carbon nanostructures is achievable via a straightforward and efficient metal-mediated alkyne cyclotrimerization reaction. We provide insight into suitable metals for this transformation, the photophysics of these trimeric molecules, as well as their strain profiles and crystal packing. We also demonstrate the strain-enhanced nature of the reaction under the optimized conditions, showing that strained internal-alkyne [*n* + 1]CPPs efficiently undergo complete conversion whereas unstrained diphenylacetylene remains completely unreacted. We anticipate that this work will have broader impacts on the study of reactivity in strained-alkyne-containing hydrocarbons, and that access to this new molecular architecture will inspire new research and applications in materials science and related fields.

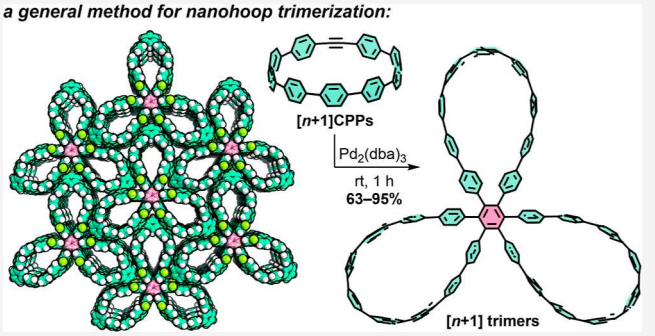

INTRODUCTION

Curved aromatic hydrocarbons are a useful and continuously evolving class of carbon nanomaterials. Their deviation from the flat, planar structure expected of aromatic molecules can grant them advantages such as (1) narrower HOMO−LUMO gaps with increasing strain,[1] (2) heightened solubility due to less efficient self-stacking,[2] and (3) complementary intermolecular interactions such as convex−concave π-interactions.[3,4] Since the landmark discoveries of fullerenes and carbon nanotubes,[5,6] many structural variants of curved aromatic hydrocarbons have been synthesized. Small molecules such as helicenes, corannulenes, saddle-shaped polyaromatics, and a variety of conjugated macrocycles are now accessible via controlled, bottom-up synthetic methods.[7] Efficient methods of derivatizing and extending these smaller fragments of curved carbon nanomaterials are crucial, as the properties and potential applications of π-rich molecules rely heavily on dimensionality, size, crystal morphology, etc. However, structural modifications of strained aromatics can be challenging, particularly due to strain-relieving pathways leading to undesired side products.

In the last several years a class of synthetically tunable curved aromatic hydrocarbons, carbon nanohoops, have garnered much attention from the broader scientific community.[7−13] Carbon nanohoops (also known as cycloparaphenylenes and abbreviated [*n*]CPP where *n* = number of phenylene units) are strained aromatic macrocycles that represent the smallest cross-section of an armchair carbon nanotube.[14] Many molecules in this class have shape-persistent pores with host−guest capabilities,[3,4] are redox active,[13,15−18] brightly fluorescent,[15] possess excellent solubility in most organic solvents,[15] and have syntheses which are highly modular and tunable; this has enabled the study of nanohoops of many different sizes, shapes, functionalities, and properties.[7−13,19]

A growing area of CPP research aims to controllably extend the strained scaffold into novel π-rich systems, such as cages, mechanically interlocked molecules, supramolecular complexes, discrete oligomers, and high molecular weight polymers.[20−24] Specifically, several recent publications have showcased the syntheses[25−30] of cycloparaphenylene-like structures with multiple hoops incorporated within one molecule (see Figure 1b for a few representative examples). The synthetic strategies of these extended CPP derivatives,

Received: September 4, 2024
Revised: October 17, 2024
Accepted: October 18, 2024
Published: October 23, 2024

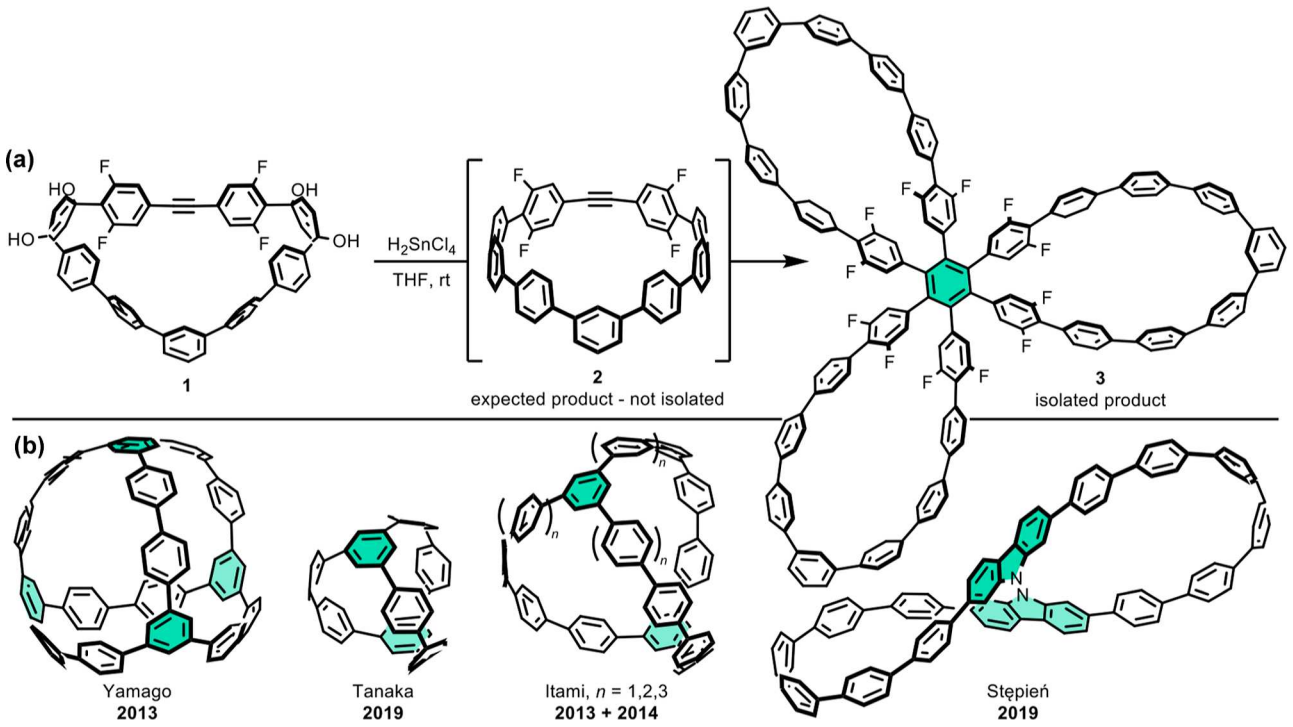

Figure 1. (a) Initial findings wherein subjection of macrocycle **1** to reductive aromatization conditions resulted not in isolation of the expected strained alkyne-containing CPP **2** but instead trimeric species **3**. (b) Previous examples of multipore nanohoop-type structures.

however, typically use early stage functionalization to build multipore precursors, which are aromatized to the final molecule often in low yield. Much less prevalent are examples of CPPs undergoing late-stage transformations, a synthetic strategy that circumvents restrictive prefunctionalization and should afford easier access to further derivation.

Our group has recently focused on the synthesis and study of [*n* + 1]CPPs,[31] wherein the "+1" refers to the incorporation of a single alkyne unit inserted in the macrocyclic backbone providing a synthetic handle for further reactivity. We have shown that these [*n* + 1]CPPs have tunable reactivity toward strain-promoted [2 + 2]cycloadditions/cycloreversions and [3 + 2]azide−alkyne cycloadditions,[31−33] but other strain-promoted transformations that may lead to multipore structures have not been reported.[33] The present work explores the [2 + 2 + 2] alkyne cyclotrimerization of a series of [*n* + 1]CPPs. While the formation of benzene derivatives via transition metal catalyzed [2 + 2 + 2] cycloaddition of alkynes has been known for over 70 years,[34] typically these reactions require elevated temperatures and long reaction times.[35] Inspired by related reactions with arynes[36,37] and small, strained cycloalkynes,[38] herein, we demonstrate the first examples of strain-promoted [2 + 2 + 2] cyclotrimerizations of alkyne-containing macrocyclic precursors to realize large, highly fluorescent, and soluble carbon nanostructures. This is a highly efficient late-stage transformation affording large curved aromatic molecules wherein three CPP fragments are linked in two dimensions around a newly formed central benzene unit (Scheme 1). Coupled with the well-established building block approach to nanohoop derivatives and the ease of preparation of most [*n* + 1]CPPs, this methodology provides access to an array of new structures that are interesting for potential applications in molecular electronics, extended supramolecular complexes, and porous carbon nanomaterials.[39]

Scheme 1. Conversion of [*n* + 1]CPPs to Trimers[a]

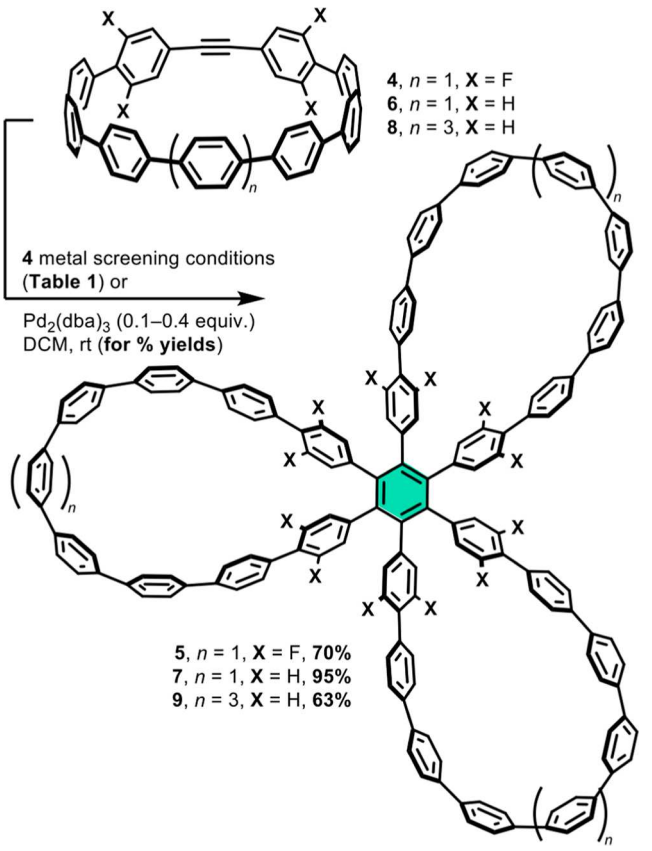

[a]**4** was chosen as a model system to assess the effectiveness of metal catalysts on the reaction (see Table 1). Percent yields refer to optimized conditions with $Pd_2(dba)_3$.

https://doi.org/10.1021/jacs.4c12272
J. Am. Chem. Soc. 2024, 146, 30607−30614

RESULTS AND DISCUSSION

Our most recent work with the [*n* + 1]CPPs focused on increasing reactivity toward the strain-promoted azide−alkyne cycloaddition reaction by (1) the introduction of electron-withdrawing fluorine atoms near the strained alkyne, and (2) the installation of a meta-linked phenylene into the nanohoop opposite the alkyne.[32] At that time we were unable to isolate the highly strained and electronically activated CPP **2** (Figure 1a) due to its propensity to decompose and/or react immediately under the reaction conditions. Gratifyingly, we were later able to identify the trimeric species **3** (Figure 1a) as one of the byproducts of the highly reactive **2**. With knowledge of the reactivities, photophysical characteristics, and host−guest capabilities of the previously synthesized [*n* + 1]CPPs in mind, we chose four species with increasingly reactive alkyne units for this study: the **8**, **6**, **4**, and **2**. We hypothesized that the transient **2** and other alkyne-containing CPPs could be efficiently trimerized with the addition of an appropriate metal catalyst.

We first focused our attention on the synthesis of the fully para-linked fluorinated internal-alkyne CPP **4** (Scheme 1) using a combination of previously described[31,32] molecular building blocks (see Supporting Information for full synthetic details). We found that **4** could be isolated effectively under the same reaction and purification conditions which had proved unsuccessful for **2**. Interestingly, we would occasionally observe slow conversion of **4** to **5** if the sample was kept as a solution in possibly metal-contaminated glassware and/or had not yet been rigorously purified. This finding, along with that of **2** forming trimer without added catalyst, suggests that the [2 + 2 + 2] alkyne trimerization of [*n* + 1]CPPs might be strain-promoted. With the comparatively more stable **4** in hand, we turned our attention to better understanding the nature of the trimerization reaction. Under inert atmosphere at room temperature with new and pristine glassware in deuterated chloroform ($CDCl_3$), we treated **4** with different metal catalysts (approximately 20% catalyst loading) for 1 h and assessed the results of each reaction with quantitative ^{19}F NMR (Table 1 and Scheme 1). The screened metal complexes are well-known catalysts for alkyne trimerization; Rh(I)[40,41] and Ni(0)[42−44] are common catalysts for the trimerization of unstrained alkynes, while Pd(0)[36,38,45] is often an effective catalyst for aryne trimerization.

Table 1. Metal Screening Results for Conversion of 4 to 5[a]

metal	conversion (%)
none	0.5
$Pd_2(dba)_3$	99.9
$RhCl(PPh_3)_3$	6.3
Ni(cod)DQ	11.5

[a]Reactions carried out in $CDCl_3$ at room temperature for 1 h under inert atmosphere with 1.9 mM **4**, 0.39 mM metal. Conversions determined by quantitative ^{19}F NMR.

We found that $Pd_2(dba)_3$ was by far the most efficient catalyst for the transformation of **4** to **5**, with a calculated percent conversion of over 99% (with these conditions, we achieved 70% isolated yield in a separate experiment). $RhCl(PPh_3)_3$ and Ni(cod)DQ performed much more modestly at 6.3% and 11.5% conversion, respectively. This apparent catalyst preference is similar to that observed by Peña et al. in their investigations of cyclohexyne trimerization.[38] Notably, we observed less than 0.5% conversion of **4** to **5** in an hour-long, room temperature control experiment with no added metal (first entry of Table 1). In a separate control experiment, we found that diphenylacetylene (an unstrained, phenyl-substituted alkyne) showed no reaction under the same conditions with $Pd_2(dba)_3$ (see Supporting Information for details). These results are consistent with our hypothesis that the cyclotrimerization of the [*n* + 1]CPPs with Pd(0) is strain-promoted. Bennett and Schwemlein have shown that cyclooctyne, the smallest isolable unsubstituted cycloalkyne, has increased complexation toward transition metal compounds compared to acyclic alkynes.[46] As a result, cyclooctyne undergoes transition metal-catalyzed cyclotrimerization far more readily than acyclic alkynes. We hypothesize that our strained alkyne-containing CPPs may also benefit from enhanced transition metal complexation, affording complete conversion to trimeric species in minutes at room temperature.

We next questioned whether less reactive [*n* + 1]CPPs could undergo cyclotrimerization under the same conditions. To assess whether electron-withdrawing fluorine atoms were necessary for the transformation, we combined **6** and catalytic $Pd_2(dba)_3$ and found that alkyne cyclotrimerization occurred efficiently to form **7** in 95% isolated yield. To investigate if less strained [*n* + 1]CPPs were also capable of this transformation, we subsequently treated **8** with $Pd_2(dba)_3$ and found that **9** could be isolated in 63% yield. While we found that **7**, **5**, and **3** all possessed excellent solubility in a range of organic solvents, **9** suffered from a lack of significant solubility in most solvents, which likely contributed to its diminished isolated yield. Despite difficulties during isolation, the crude NMR of the trimerization of **8** shows clean and complete conversion to **9**.

Finally, we turned our attention back to a more efficient synthesis of **3**. After testing several methods, we found that we could reliably form **3** by adding 1.5 equiv of Ni(cod)DQ directly to the reductive aromatization reaction of **2**. This allowed us to form **3** in up to 52% yield from **1** after purification.

We confirmed the identity and connectivity of **3** and **5** via X-ray crystal analysis (unit cells shown in Figure 2). Crystals of **5** were formed from the slow evaporation of 1,4-dioxane. Crystals of **3** were formed from vapor diffusion of pentanes into 1,4-dioxane. In both cases, precise structural information could not be determined due to a high number of disordered solvent molecules. However, the X-ray data was sufficient to confirm the correct assignment of both molecules and assign a space group ($P\bar{1}$ for **5** and *R*3 for **3**) for each crystal packing pattern. Notably, **3** packs into an interdigitated structure with long-range, solvent-filled channels.

While we were not able to grow suitable single crystals of **7** and **9**, spectroscopic evidence is consistent with the structural assignment. Figure 3 shows the ^1H NMR spectra in deuterated dichloromethane (DCM) (CD_2Cl_2) for each of the trimers described herein as well as relevant [*n* + 1]CPPs. For [*n* + 1]CPPs, we typically observe a distinctive upfield doublet representative of the hydrogens ortho to the alkyne (shown generically as H_A in Figure 3).[31,32] For nonfluorinated **7** and **9**, another upfield doublet, likely representative of the hydrogens meta to the alkyne (H_B in Figure 3), can also be observed. Upon trimerization of **4**, an upfield shift of the H_A doublet occurred from 6.96 ([*n* + 1]CPP) to 6.65 ppm (trimer). Notably, the H_A doublets of **6** and **8** experience very comparable shifts upon trimerization (7.36 to 6.99 ppm for **6** to **7**, and 7.45 to 7.05 ppm for **8** to **9**). In these cases, we can

https://doi.org/10.1021/jacs.4c12272
J. Am. Chem. Soc. 2024, 146, 30607−30614

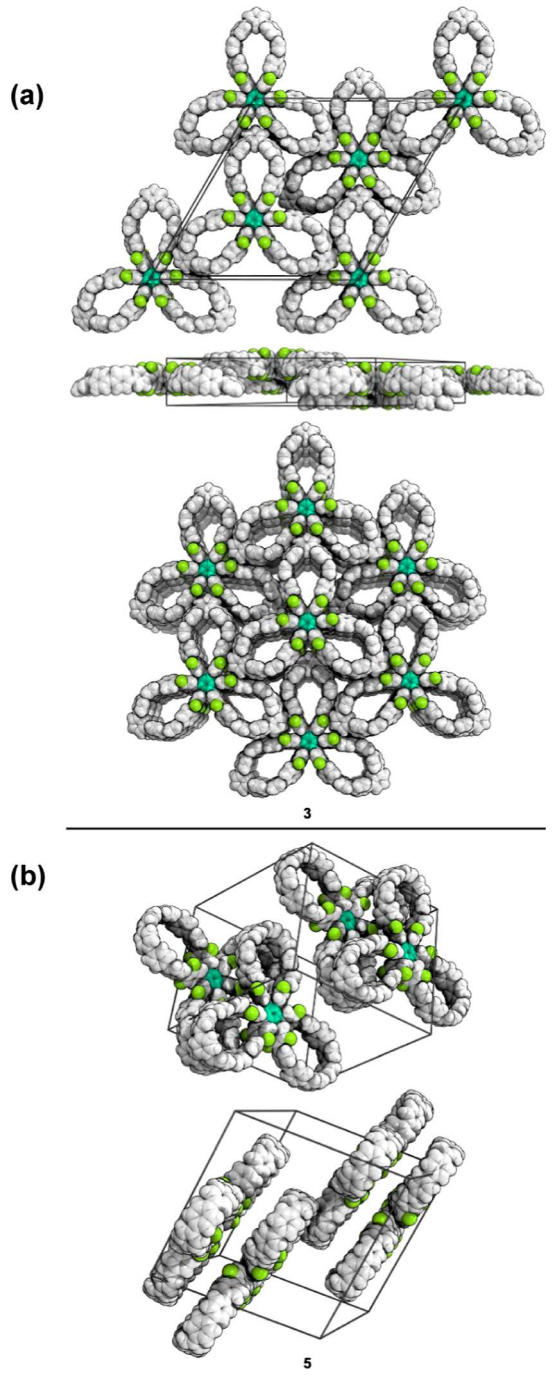

Figure 2. X-ray crystal structure unit cells of (a) **3** and (b) **5**. Solvent omitted for clarity.

also note the upfield shift of the H_B signal; the doublet representing H_B shifts from 7.50 ppm for **6** to 7.20 ppm for **7**, and from 7.57 ppm for **8** to 7.26 ppm for **9**. Further NMR evidence for successful trimerization can be found in the ^{13}C NMR (see Supporting Information for full details). In these spectra, we see a disappearance of any signals below 120 ppm, indicating the lack of an alkyne in the product (the alkyne signals for **4**, **6**, and **8** in CD_2Cl_2 are observed at 99.24, 99.39, and 97.10 ppm, respectively). In addition to NMR spectroscopic evidence, high resolution mass spectrometry of **3**, **5**, **7**, and **9** resulted in the correct ion masses.

We next worked to better understand the total strain and distribution of local strain in these new nanohoop derivatives.

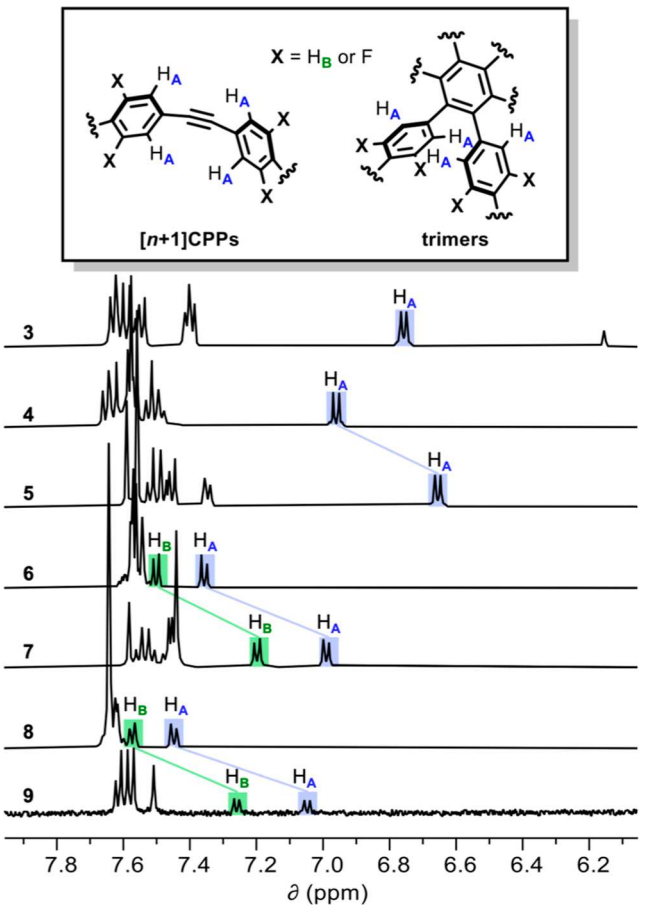

Figure 3. Diagnostic ^1H NMR shifts for trimers and associated [n + 1]CPPs in CD_2Cl_2.

We used the computational program StrainViz to calculate and visualize the local and total strain of each trimer and its parent [n + 1]CPP (Table 2 and Figure 4).[48] For the [n + 1]CPPs,

Table 2. Quantitative Strain Data as Determined by StrainViz (All Values in kcal mol^{-1})[a]

compound	max. local strain	total strain
3	1.8	80.5
5	3.1	130.3
7	3.1	129.3
9	2.3	112.8
2	3.4	42.9
4	2.8	55.6
6	2.9	58.0
8	1.3	44.4

[a]Computations performed with Gaussian 09 at the B3LYP/6-31G(d) level of theory.[47]

local strain is greatest at the alkyne as has been shown previously.[32,48] For the trimers, however, local strain is greatest at the phenylene units opposite the newly formed ortho linkage—this is consistent with our understanding of how strain is distributed in these types of macrocycles.[48] Additionally, the trimmers have total strain values equivalent to less than three times the total strain of the precursor [n + 1]CPPs. For example, **5** has a calculated 130 kcal mol^{-1} of inherent strain, whereas **4** has 56 kcal mol^{-1}. These findings indicate that the inherent strain per macrocyclic unit decreases post-

https://doi.org/10.1021/jacs.4c12272
J. Am. Chem. Soc. 2024, 146, 30607−30614

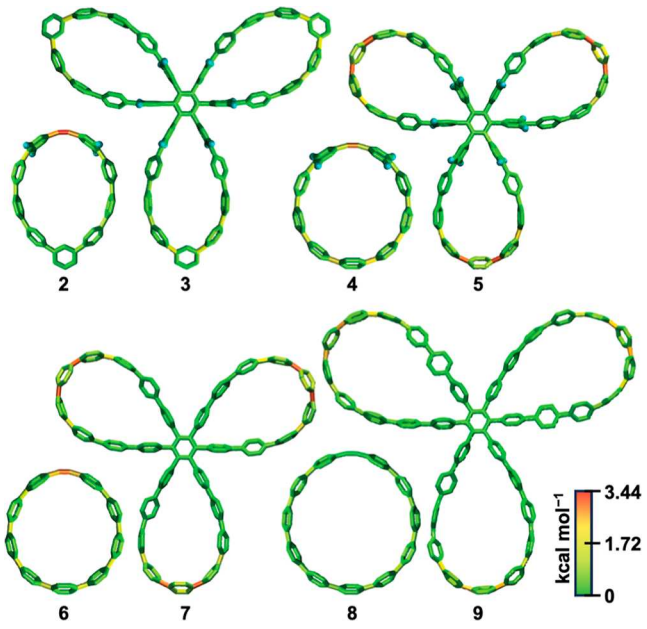

Figure 4. StrainViz structures for each trimer and its respective [*n* + 1]CPP (**2** was not isolated but is shown here for completeness).

trimerization. We also note that **2**, which has the highest calculated maximum local strain value of the [*n* + 1]CPPs in this study at 3.4 kcal mol^{-1}, trimerizes to form the most locally and globally unstrained trimer in this series, **3**. The meta linkage serves to heighten strain in nanohoops at the region of the molecule directly across from it,[48] but post-trimerization the newly formed ortho-linkage ameliorates this effect.

Photophysical data for each trimer and its associated parent [*n* + 1]CPP[31,32] (where applicable) are displayed in Figure 5 and Table 3. Absorbance and emission traces as well as quantum yields were collected for all molecules in comparatively nonpolar DCM and polar dimethyl sulfoxide (DMSO) to probe any solvent-dependent effects; extinction coefficients were collected in DCM. For all but one of the trimers, we did not observe a large solvent effect on photophysics beyond a slight red-shifting in maximum absorbance wavelength ($\lambda_{max,abs}$) and maximum emission wavelength ($\lambda_{max,em}$) values in DMSO (Table 3 and Figure 5c). Therefore, we focused our analysis of trimer photophysics on the measured values in DCM. The only notable solvent effects were observed for **fluor[9 + 1]CPP**, which displayed highly solvent-dependent fluorescence properties (vide infra).

Carbon nanohoops typically display a $\lambda_{max,abs}$ around 340 nm. This major absorbance band is dominated by degenerate HOMO − 2/HOMO − 1 to LUMO and HOMO to LUMO + 1/LUMO + 2 transitions, as the HOMO to LUMO transition is symmetry forbidden in most cases.[15,49]

When comparing the absorbance profiles of each trimer to its parent [*n* + 1]CPP, we can observe a slight hypsochromic shift of $\lambda_{max,abs}$ upon trimerization. For example, **6** has a measured $\lambda_{max,abs}$ of 342 nm in DCM, while **7** has a slightly blue-shifted $\lambda_{max,abs}$ of 337 nm. Nonetheless, **5**, **7**, and **9** all maintain $\lambda_{max,abs}$ values around the typical 340 nm. Computational results for **5** (Supporting Information Table S9) indicate that the HOMO−LUMO transition is weak, and the stronger absorption is a combination of higher energy transitions (e.g., HOMO to LUMO + 3, HOMO to LUMO + 4, etc.). Comparing the trimers, we note that **5** has a slightly blue-shifted $\lambda_{max,abs}$ compared to **7**. We have previously observed a slight hypsochromic shift in fluorinated para-linked nanohoops compared to their hydrocarbon counterparts.[32,50,51] Finally, the shortest wavelength $\lambda_{max,abs}$ is displayed by **3**; we hypothesize that the significant lack of strain in this molecule in comparison to the other trimers elevates the energy of this transition.[52]

The extinction coefficient for each trimer is plotted as a function of wavelength in Figure 5a; extinction coefficients for each trimer (and corresponding [*n* + 1]CPP) at $\lambda_{max,abs}$ are displayed in Table 3. In each case where it is possible to compare the trimer to its [*n* + 1]CPP parent, we observe that the extinction coefficient at $\lambda_{max,abs}$ is (within error) approximately three times that of the parent. For instance, we previously measured an extinction coefficient for **6** of 1.55 × 10^5 M^{-1} cm^{-1} in DCM at $\lambda_{max,abs}$.[31] This value essentially triples for **7** with a measured extinction coefficient of 4.52 × 10^5 M^{-1} cm^{-1}. This is an intriguing result which suggests that the molar absorptivity of each [*n* + 1]CPP macrocycle is maintained even upon its incorporation into the trimeric species, establishing the [*n* + 1] trimers as exceptionally bright chromophores.

The fluorescence emission traces for each trimer are plotted in Figure 5a as a function of wavelength and normalized such that the maximum *y*-axis value matches the molecule's measured quantum yield in DCM. We observe that **9**, **5**, and **7** display fluorescence emissions that are slightly red-shifted in comparison to their parent [*n* + 1]CPPs; for example, the maximum emission wavelength ($\lambda_{max,em}$) for **6** in DCM was previously measured to be 463 nm,[31] while **7** displays a $\lambda_{max,em}$ of 472 nm. As is generally observed in carbon nanohoops,[15]

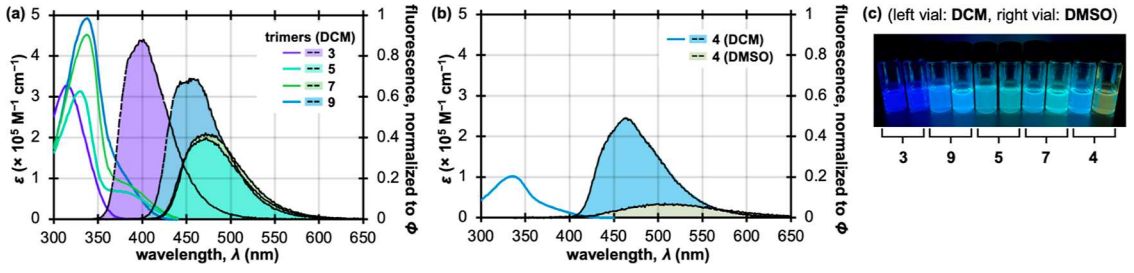

Figure 5. Photophysical characterization for the new molecules described herein. (a) Extinction coefficients (colored lines) and fluorescence emission traces (black lines) for each trimer in DCM plotted as a function of wavelength. Fluorescence traces are scaled such that the maximum *y*-value of each curve matches the quantum yield of the compound in DCM. (b) Extinction coefficient for **4** (blue line) as a function of wavelength in DCM plotted along with fluorescence emission traces (black lines) for **4** in DCM and DMSO (emission curves are also scaled to quantum yield in the respective solvent). (c) Solutions of trimers and **4** in DCM and DMSO under irradiation with long-wave UV light.

https://doi.org/10.1021/jacs.4c12272
J. Am. Chem. Soc. 2024, 146, 30607−30614

Table 3. Tabulated Photophysical Data for Trimers and Associated [n + 1]CPPs[a]

compound	$\lambda_{max,abs}$ (nm)		$\lambda_{max,em}$ (nm)		extinction coefficient, ε ($\times 10^5$ M^{-1} cm^{-1})	quantum yield, Φ	
	DCM	DMSO	DCM	DMSO	DCM	DCM	DMSO
3	315	318	402	415	3.27 ± 0.04	0.88	0.88
4	335	343	463	507	1.02 ± 0.04	0.49	0.07
5	330	337	472	479	3.13 ± 0.23	0.40	0.46
6	342	351	463	473	1.55	0.76	0.67
7	337		472	487	4.52 ± 0.07	0.42	0.47
8	341	350	449	460	1.63	0.80	0.83
9	338		454	468	4.93 ± 0.20	0.69	0.67

[a]Values for **6** and **8** were measured previously[24,25] and included here as a point of reference. Note that quantum yields were measured by slightly different methods than were used in this study (see Supporting Information and previous publications for details).

the smaller **7** and **5** have a red-shifted emission in comparison to the larger **9**, probably due to increased conjugation between phenylenes in smaller sizes. We observe that fluorination of scaffold of **7** does not seem to significantly affect fluorescence properties. The hypsochromic fluorescence emission of **3** in comparison to the other trimers in this study can most likely be attributed to a lack of strain in the molecule which in turn decreases p-orbital overlap and widens the HOMO−LUMO gap.[15,52] Quantum yields for all trimers were reasonably high: **5** and **7** displayed quantum yields of 0.40 and 0.42 in DCM, respectively, while the larger **9** displayed a slightly higher quantum yield of 0.69. **3** exhibited the highest quantum yield in the series at 0.88.

Figure 5b,c highlight the significant solvent-dependent fluorescence properties of **4**. The $\lambda_{max,em}$ for **4** shifts from 463 nm in DCM to 507 nm in DMSO. This bathochromic shift in $\lambda_{max,em}$ with increasing solvent polarity is accompanied by a notable drop in quantum yield from 0.49 in DCM to 0.07 in DMSO. These results suggest that **4** is a donor−acceptor-type nanohoop that, upon excitation, experiences charge transfer from the electron-rich curved phenylene backbone of the nanohoop to the electron-poor, fluorinated, alkyne-containing region[13,16,17,32,53−56] (see Supporting Information Figure S39 for further details). We speculate that a polarized excited state would be better stabilized in polar solvents such as DMSO, therefore resulting in a lower energy transition back to the ground state and longer wavelength $\lambda_{max,em}$.[57] The lower quantum yield would in turn be explained by the energy gap law, as has been seen previously for donor−acceptor molecules.[58] The fact that the quantum yield in DMSO is largely restored upon trimerization to **5** suggests that the trimer's excited state is significantly less polarized.[57,58] This finding is consistent with our calculations (see Supporting Information Figure S39).

CONCLUSION

Employing suitable late-stage transformations of curved aromatic hydrocarbons is a promising approach for systematically diversifying their structures, and in turn, their applications. The realization of unique molecular architectures is a major driving force for uncovering and characterizing the rich structure function relationships that render organic synthesis a tool for advancing carbon nanoscience. Our previous studies of strained alkyne-containing carbon nanohoops focused on efficiently attaching them via click chemistry methods to other small molecules of interest.[31−33] In this work, we have described a synthetically simple and high yielding method for expanding these molecules into larger carbon nanostructures by a metal-catalyzed trimerization reaction. The result is high molecular weight pinwheel-shaped [n + 1] trimers with exceptionally high luminescence and generally good solubility. We envision that this method can provide access to trimer derivatives with unique photophysics, structure, and functionality, especially given the modularity of [n + 1]CPP syntheses. For example, the inclusion of donor and acceptor groups to tune optoelectronic properties, functional handles as sites for further reactivity, and heteroatoms to tune supramolecular capabilities are all accessible and exciting next steps for these trimeric macrocycles. The current work also provides further evidence that strained alkyne nanohoops are amenable to derivatization through a variety of metal-mediated reactions; classical work of Reppe et al. suggests that the use of an appropriate transition metal catalyst may afford tetrameric species with four CPPs linked around a newly formed cyclooctatetraene.[34] The use of strain promoted reactions to generate well-defined carbon nanomaterials is an exciting area of research lying at the interface of organic synthesis and nanoscience that we will continue to explore.

ASSOCIATED CONTENT

Supporting Information

The Supporting Information is available free of charge at https://pubs.acs.org/doi/10.1021/jacs.4c12272.

Experimental and computational procedures, spectral data, and crystallographic information (PDF)

Accession Codes

Deposition numbers 2334369−2334370 contain the supplementary crystallographic data for this paper. These data can be obtained free of charge via the joint Cambridge Crystallographic Data Centre (CCDC) and Fachinformationszentrum Karlsruhe Access Structures service.

AUTHOR INFORMATION

Corresponding Author

Ramesh Jasti − *Department of Chemistry and Biochemistry, Materials Science Institute, and Knight Campus for Accelerating Scientific Impact, University of Oregon, Eugene, Oregon 97403, United States;* orcid.org/0000-0002-8606-6339; Email: rjasti@uoregon.edu

Authors

Tara D. Clayton − *Department of Chemistry and Biochemistry, Materials Science Institute, and Knight Campus for Accelerating Scientific Impact, University of Oregon, Eugene, Oregon 97403, United States*

Julia M. Fehr − *Department of Chemistry and Biochemistry, Materials Science Institute, and Knight Campus for Accelerating Scientific Impact, University of Oregon, Eugene, Oregon 97403, United States;* orcid.org/0000-0001-8426-3032

Tavis W. Price − *Department of Chemistry and Biochemistry, Materials Science Institute, and Knight Campus for Accelerating Scientific Impact, University of Oregon, Eugene, Oregon 97403, United States;* orcid.org/0000-0002-4803-9233

Lev N. Zakharov − *CAMCOR—Center for Advanced Materials Characterization in Oregon, University of Oregon, Eugene, Oregon 97403, United States*

Complete contact information is available at: https://pubs.acs.org/10.1021/jacs.4c12272

Author Contributions

[§]T.D.C. and J.M.F. contributed equally to this work.

Notes

The authors declare no competing financial interest.

■ ACKNOWLEDGMENTS

We would like to acknowledge the National Science Foundation (NSF) grant number NSF-CHE-2102567 and NSF-CHE-2400147. This work benefited from the Oregon high performance computer, Talapas.

■ REFERENCES

(1) Scott, L. T.; Bronstein, H. E.; Preda, D. V.; Ansems, R. B. M.; Bratcher, M. S.; Hagen, S. Geodesic Polyarenes with Exposed Concave Surfaces. *Pure Appl. Chem.* **1999**, *71* (2), 209−219.

(2) Bheemireddy, S. R.; Ubaldo, P. C.; Finke, A. D.; Wang, L.; Plunkett, K. N. Contorted Aromatics via a Palladium-Catalyzed Cyclopentannulation Strategy. *J. Mater. Chem. C* **2016**, *4* (18), 3963−3969.

(3) Xu, Y.; Kaur, R.; Wang, B.; Minameyer, M. B.; Gsänger, S.; Meyer, B.; Drewello, T.; Guldi, D. M.; von Delius, M. Concave−Convex $\pi-\pi$ Template Approach Enables the Synthesis of [10]-Cycloparaphenylene−Fullerene [2]Rotaxanes. *J. Am. Chem. Soc.* **2018**, *140* (41), 13413−13420.

(4) Ball, M.; Zhong, Y.; Fowler, B.; Zhang, B.; Li, P.; Etkin, G.; Paley, D. W.; Decatur, J.; Dalsania, A. K.; Li, H.; Xiao, S.; Ng, F.; Steigerwald, M. L.; Nuckolls, C. Macrocyclization in the Design of Organic N-Type Electronic Materials. *J. Am. Chem. Soc.* **2016**, *138* (39), 12861−12867.

(5) Iijima, S. Helical Microtubules of Graphitic Carbon. *Nature* **1991**, *354* (6348), 56−58.

(6) Kroto, H. W.; Heath, J. R.; O'Brien, S. C.; Curl, R. F.; Smalley, R. E. C60: Buckminsterfullerene. *Nature* **1985**, *318* (6042), 162−163.

(7) Majewski, M. A.; Stępień, M. Bowls, Hoops, and Saddles: Synthetic Approaches to Curved Aromatic Molecules. *Angew. Chem., Int. Ed.* **2019**, *58* (1), 86−116.

(8) Lewis, S. E. Cycloparaphenylenes and Related Nanohoops. *Chem. Soc. Rev.* **2015**, *44* (8), 2221−2304.

(9) Wu, D.; Cheng, W.; Ban, X.; Xia, J. Cycloparaphenylenes (CPPs): An Overview of Synthesis, Properties, and Potential Applications. *Asian J. Org. Chem.* **2018**, *7* (11), 2161−2181.

(10) Yamago, S.; Kayahara, E. Synthesis and Reactions of Carbon Nanohoop. *J. Synth. Org. Chem., Jpn.* **2019**, *77* (11), 1147−1158.

(11) Xu, Y.; von Delius, M. The Supramolecular Chemistry of Strained Carbon Nanohoops. *Angew. Chem., Int. Ed.* **2020**, *59* (2), 559−573.

(12) Li, Y.; Kono, H.; Maekawa, T.; Segawa, Y.; Yagi, A.; Itami, K. Chemical Synthesis of Carbon Nanorings and Nanobelts. *Acc. Mater. Res.* **2021**, *2* (8), 681−691.

(13) Hermann, M.; Wassy, D.; Esser, B. Conjugated Nanohoops Incorporating Donor, Acceptor, Hetero- or Polycyclic Aromatics. *Angew. Chem., Int. Ed.* **2021**, *60* (29), 15743−15766.

(14) Jasti, R.; Bhattacharjee, J.; Neaton, J. B.; Bertozzi, C. R. Synthesis, Characterization, and Theory of [9]-[12]-and [18]-Cycloparaphenylene: Carbon Nanohoop Structures. *J. Am. Chem. Soc.* **2008**, *130* (52), 17646−17647.

(15) Darzi, E. R.; Jasti, R. The Dynamic, Size-Dependent Properties of [5]−[12]Cycloparaphenylenes. *Chem. Soc. Rev.* **2015**, *44* (18), 6401−6410.

(16) Darzi, E. R.; Hirst, E. S.; Weber, C. D.; Zakharov, L. N.; Lonergan, M. C.; Jasti, R. Synthesis, Properties, and Design Principles of Donor−Acceptor Nanohoops. *ACS Cent. Sci.* **2015**, *1* (6), 335−342.

(17) Van Raden, J. M.; Darzi, E. R.; Zakharov, L. N.; Jasti, R. Synthesis and Characterization of a Highly Strained Donor−Acceptor Nanohoop. *Org. Biomol. Chem.* **2016**, *14* (24), 5721−5727.

(18) Narita, N.; Kurita, Y.; Osakada, K.; Ide, T.; Kawai, H.; Tsuchido, Y. A Dodecamethoxy[6]Cycloparaphenylene Consisting Entirely of Hydroquinone Ethers: Unveiling in-Plane Aromaticity through a Rotaxane Structure. *Nat. Commun.* **2023**, *14* (1), 8091.

(19) Leonhardt, E. J.; Jasti, R. Emerging Applications of Carbon Nanohoops. *Nat. Rev. Chem* **2019**, *3* (12), 672−686.

(20) Li, K.; Xu, Z.; Deng, H.; Zhou, Z.; Dang, Y.; Sun, Z. Dimeric Cycloparaphenylenes with a Rigid Aromatic Linker. *Angew. Chem., Int. Ed.* **2021**, *60* (14), 7649−7653.

(21) Yang, Y.; Blacque, O.; Sato, S.; Juríček, M. Cycloparaphenylene−Phenalenyl Radical and Its Dimeric Double Nanohoop. *Angew. Chem., Int. Ed.* **2021**, *60* (24), 13529−13535.

(22) May, J. H.; Fehr, J. M.; Lorenz, J. C.; Zakharov, L.; Jasti, R. A High-Yielding Active Template Click Reaction (AT-CuAAC) for the Synthesis of Mechanically Interlocked Nanohoops. *Angew. Chem., Int. Ed.* n/a (2024, *63*, 20), e202401823. DOI: .

(23) Zhao, C.; Meng, H.; Nie, M.; Wang, X.; Cai, Z.; Chen, T.; Wang, D.; Wang, C.; Wang, T. Supramolecular Complexes of C80-Based Metallofullerenes with [12]Cycloparaphenylene Nanoring and Altered Property in a Confined Space. *J. Phys. Chem. C* **2019**, *123* (19), 12514−12520.

(24) Maust, R. L.; Li, P.; Shao, B.; Zeitler, S. M.; Sun, P. B.; Reid, H. W.; Zakharov, L. N.; Golder, M. R.; Jasti, R. Controlled Polymerization of Norbornene Cycloparaphenylenes Expands Carbon Nanomaterials Design Space. *ACS Cent. Sci.* **2021**, *7* (6), 1056−1065.

(25) Kayahara, E.; Iwamoto, T.; Takaya, H.; Suzuki, T.; Fujitsuka, M.; Majima, T.; Yasuda, N.; Matsuyama, N.; Seki, S.; Yamago, S. Synthesis and Physical Properties of a Ball-like Three-Dimensional π-Conjugated Molecule. *Nat. Commun.* **2013**, *4* (1), 2694.

(26) Hayase, N.; Nogami, J.; Shibata, Y.; Tanaka, K. Synthesis of a Strained Spherical Carbon Nanocage by Regioselective Alkyne Cyclotrimerization. *Angew. Chem., Int. Ed.* **2019**, *58* (28), 9439−9442.

(27) Matsui, K.; Segawa, Y.; Namikawa, T.; Kamada, K.; Itami, K. Synthesis and Properties of All-Benzene Carbon Nanocages: A Junction Unit of Branched Carbon Nanotubes. *Chem. Sci.* **2013**, *4* (1), 84−88.

(28) Matsui, K.; Segawa, Y.; Itami, K. All-Benzene Carbon Nanocages: Size-Selective Synthesis, Photophysical Properties, and Crystal Structure. *J. Am. Chem. Soc.* **2014**, *136* (46), 16452−16458.

(29) Senthilkumar, K.; Kondratowicz, M.; Lis, T.; Chmielewski, P. J.; Cybińska, J.; Zafra, J. L.; Casado, J.; Vives, T.; Crassous, J.; Favereau, L.; Stępień, M. Lemniscular [16]Cycloparaphenylene: A Radially Conjugated Figure-Eight Aromatic Molecule. *J. Am. Chem. Soc.* **2019**, *141* (18), 7421−7427.

(30) Zhou, Q.; Xu, Z.; Li, K.; Tian, X.; Ye, L.; Sun, Z. Synthesis and Properties of a Strained Triple Nanohoop. *Chem.—Asian J.* **2024**, *19* (15), No. e202301131.

(31) Schaub, T. A.; Margraf, J. T.; Zakharov, L.; Reuter, K.; Jasti, R. Strain-Promoted Reactivity of Alkyne-Containing Cycloparaphenylenes. *Angew. Chem., Int. Ed.* **2018**, *57* (50), 16348−16353.

(32) Fehr, J. M.; Myrthil, N.; Garrison, A. L.; Price, T. W.; Lopez, S. A.; Jasti, R. Experimental and Theoretical Elucidation of SPAAC

Kinetics for Strained Alkyne-Containing Cycloparaphenylenes. *Chem. Sci.* **2023**, *14* (11), 2839−2848.
(33) Schaub, T. A.; Zieleniewska, A.; Kaur, R.; Minameyer, M.; Yang, W.; Schüßlbauer, C. M.; Zhang, L.; Freiberger, M.; Zakharov, L. N.; Drewello, T.; Dral, P. O.; Guldi, D. M.; Jasti, R. Tunable Macrocyclic Polyparaphenylene Nanolassos via Copper-Free Click Chemistry. *Chem.—Eur. J.* **2023**, *29* (33), No. e202300668.
(34) Reppe, W.; Schlichting, O.; Klager, K.; Toepel, T. Cyclisierende Polymerisation von Acetylen I Über Cyclooctatetraen. *Justus Liebigs Ann. Chem.* **1948**, *560* (1), 1−92.
(35) Kotha, S.; Brahmachary, E.; Lahiri, K. Transition Metal Catalyzed [2 + 2+2] Cycloaddition and Application in Organic Synthesis. *Eur. J. Org Chem.* **2005**, *2005* (22), 4741−4767.
(36) Peña, D.; Escudero, S.; Pérez, D.; Guitián, E.; Castedo, L. Efficient Palladium-Catalyzed Cyclotrimerization of Arynes: Synthesis of Triphenylenes. *Angew. Chem., Int. Ed.* **1998**, *37* (19), 2659−2661.
(37) Radhakrishnan, K. V.; Yoshikawa, E.; Yamamoto, Y. Palladium Catalyzed Co-Trimerization of Benzyne with Alkynes. A Facile Method for the Synthesis of Phenanthrene Derivatives. *Tetrahedron Lett.* **1999**, *40* (42), 7533−7535.
(38) Peña, D.; Pérez, D.; Guitián, E. Cyclotrimerization Reactions of Arynes and Strained Cycloalkynes. *Chem. Rec.* **2007**, *7* (6), 326−333.
(39) Vij, V.; Bhalla, V.; Kumar, M. Hexaarylbenzene Evolution of Properties and Applications of Multitalented Scaffold. *Chem. Rev.* **2016**, *116* (16), 9565−9627.
(40) Tanaka, K. Rhodium-Mediated [2 + 2 + 2] Cycloaddition. In *Transition-Metal-Mediated Aromatic Ring Construction*; John Wiley & Sons, Ltd, 2013; pp 127−160.
(41) Pla-Quintana, A.; Roglans, A. The Choice of Rhodium Catalysts in [2 + 2+2] Cycloaddition Reaction: A Personal Account. *Molecules* **2022**, *27* (4), 1332.
(42) Kumar, P.; Louie, J. Nickel-Mediated [2 + 2 + 2] Cycloaddition. In *Transition-Metal-Mediated Aromatic Ring Construction*; John Wiley & Sons, Ltd, 2013; pp 37−70.
(43) Stará, I. G.; Starý, I.; Kollárovič, A.; Teplý, F.; Vyskočil, Š.; Šaman, D. Transition Metal Catalysed Synthesis of Tetrahydro Derivatives of [5]-, [6]- and [7]Helicene. *Tetrahedron Lett.* **1999**, *40* (10), 1993−1996.
(44) Teplý, F.; Stará, I. G.; Starý, I.; Kollárovič, A.; Šaman, D.; Rulíšek, L.; Fiedler, P. Synthesis of [5]-[6]-and [7]Helicene via Ni(0)- or Co(I)-Catalyzed Isomerization of Aromatic Cis,Cis-Dienetriynes. *J. Am. Chem. Soc.* **2002**, *124* (31), 9175−9180.
(45) Kotha, S.; Brahmachary, E.; Lahiri, K. Transition Metal Catalyzed [2 + 2+2] Cycloaddition and Application in Organic Synthesis. *Eur. J. Org Chem.* **2005**, *2005* (22), 4741−4767.
(46) Bennett, M. A.; Schwemlein, H. P. Metal Complexes of Small Cycloalkynes and Arynes. *Angew Chem. Int. Ed. Engl.* **1989**, *28* (10), 1296−1320.
(47) Gaussian 09 CitationlGaussian.com. https://gaussian.com/g09citation/ (accessed Oct 28, 2022).
(48) Colwell, C. E.; Price, T. W.; Stauch, T.; Jasti, R. Strain Visualization for Strained Macrocycles. *Chem. Sci.* **2020**, *11* (15), 3923−3930.
(49) Adamska, L.; Nayyar, I.; Chen, H.; Swan, A. K.; Oldani, N.; Fernandez-Alberti, S.; Golder, M. R.; Jasti, R.; Doorn, S. K.; Tretiak, S. Self-Trapping of Excitons, Violation of Condon Approximation, and Efficient Fluorescence in Conjugated Cycloparaphenylenes. *Nano Lett.* **2014**, *14* (11), 6539−6546.
(50) Leonhardt, E. J.; Van Raden, J. M.; Miller, D.; Zakharov, L. N.; Alemán, B.; Jasti, R. A. A Bottom-Up Approach to Solution-Processed, Atomically Precise Graphitic Cylinders on Graphite. *Nano Lett.* **2018**, *18* (12), 7991−7997.
(51) Van Raden, J. M.; Leonhardt, E. J.; Zakharov, L. N.; Pérez-Guardiola, A.; Pérez-Jiménez, A. J.; Marshall, C. R.; Brozek, C. K.; Sancho-García, J. C.; Jasti, R. Precision Nanotube Mimics via Self-Assembly of Programmed Carbon Nanohoops. *J. Org. Chem.* **2020**, *85* (1), 129−141.
(52) Lovell, T. C.; Colwell, C. E.; Zakharov, L. N.; Jasti, R. Symmetry Breaking and the Turn-on Fluorescence of Small, Highly Strained Carbon Nanohoops. *Chem. Sci.* **2019**, *10* (13), 3786−3790.
(53) Chen, D.; Wada, Y.; Kusakabe, Y.; Sun, L.; Kayahara, E.; Suzuki, K.; Tanaka, H.; Yamago, S.; Kaji, H.; Zysman-Colman, E. A Donor−Acceptor 10-Cycloparaphenylene and Its Use as an Emitter in an Organic Light-Emitting Diode. *Org. Lett.* **2023**, *25* (6), 998−1002.
(54) Kuwabara, T.; Orii, J.; Segawa, Y.; Itami, K. Curved Oligophenylenes as Donors in Shape-Persistent Donor−Acceptor Macrocycles with Solvatofluorochromic Properties. *Angew. Chem., Int. Ed.* **2015**, *54* (33), 9646−9649.
(55) Lovell, T. C.; Garrison, Z. R.; Jasti, R. Synthesis, Characterization, and Computational Investigation of Bright Orange-Emitting Benzothiadiazole [10]Cycloparaphenylene. *Angew. Chem., Int. Ed.* **2020**, *59* (34), 14363−14367.
(56) Bliksted Roug Pedersen, V.; Price, T. W.; Kofod, N.; Zakharov, L. N.; Laursen, B. W.; Jasti, R.; Brøndsted Nielsen, M. Synthesis and Properties of Fluorenone-Containing Cycloparaphenylenes and Their Late-Stage Transformation. *Chem.—Eur. J.* **2024**, *30* (5), No. e202303490.
(57) Barnsley, J. E.; Shillito, G. E.; Mapley, J. I.; Larsen, C. B.; Lucas, N. T.; Gordon, K. C. Walking the Emission Tightrope: Spectral and Computational Analysis of Some Dual-Emitting Benzothiadiazole Donor−Acceptor Dyes. *J. Phys. Chem. A* **2018**, *122* (40), 7991−8006.
(58) Caspar, J. V.; Meyer, T. J. Application of the Energy Gap Law to Nonradiative, Excited-State Decay. *J. Phys. Chem.* **1983**, *87* (6), 952−957.

https://doi.org/10.1021/jacs.4c12272
J. Am. Chem. Soc. 2024, 146, 30607−30614